Synthesis and Characterization of Colorimetric Metal Sensing Properties Based on Azo Chromophore Moiety

Young-A Son [a] , Young-Sung Kim [a] , Sung-Hoon Kim [b] & Do-Hyun Lee [c]

[a] Department of Advanced Organic Materials and Textile System Engineering, Chungnam National University, Daejeon, S. Korea

[b] Department of Textile System Engineering, Kyungpook National University, Daegu, S. Korea

[c] Korea Dyeing Research & Technology Center, S. Korea

Version of record first published: 16 May 2011

PLEASE SCROLL DOWN FOR ARTICLE

Taylor & Francis
Taylor & Francis Group

Synthesis and Characterization of Colorimetric Metal Sensing Properties Based on Azo Chromophore Moiety

YOUNG-A SON,[1] YOUNG-SUNG KIM,[1]
SUNG-HOON KIM,[2] AND DO-HYUN LEE[3]

[1]Department of Advanced Organic Materials and Textile System Engineering, Chungnam National University, Daejeon, S. Korea
[2]Department of Textile System Engineering, Kyungpook National University, Daegu, S. Korea
[3]Korea Dyeing Research & Technology Center, S. Korea

In this work, we have designed and synthesized a particular colorimetric dye sensor for the detection of heavy metal ions. Dye sensor, namely 4-hydroxy-3-(fluoro-phenyl-thiourea-N'-nitrilo-methylidynyl)-azobenzene was synthesized using 5-phenyldiazenyl salicylaldehyde and 4-phenylthiosemi carbazide. The dye sensor has promising properties which are applicable to detect and recognize the presence of heavy metal ions with colorimetric changing functions. Electron rich part in dye sensor structure, which can be utilized as metal binding unit, such as NH, N, S and OH (atom/group) provides the functions to coordinate metal ions. This metal ion detection property was determined by using UV-Vis absorption, ¹H-NMR peak shift and computational calculation method analysis. Furthermore, we estimated the electrochemical properties of dye sensor by using cyclicvoltammetry. In addition, the formation type of metal binding complex was determined by Job's plot measurements.

Keywords Absorption; azo chromophore; colorimetric sensing; dye sensor; heavy metal ion; HOMO/LUMO

1. Introduction

Recently, dye sensor researches have received much attention due to detection properties of harmful materials such as heavy metal ions. Dye sensors for specific chemicals are based on metal complex ligands such as crown ether, cryptand and spherand in the structures. Many interesting works have been carried out for detection of heavy metal ions [1–4]. In the context of biological and environmental aspects, heavy metal ions are considered to be highly dangerous in the human body [5,6]. Thus, the design of effective dye sensors and their utilizations over heavy metal

Address correspondence to Young-A Son, Department of Advanced Organic Materials, and Textile System Engineering, Chungnam National University, Daejeon, 305-764, S. Korea. Tel.: +82 42 821 6620; Fax: +82 42 823 3736; E-mail: yason@cnu.ac.kr or Sung-Hoon Kim, Department of Textile System Engineering, Kyungpook National University, Daegu, 702-701, S. Korea. Tel.: +82 53 950 5641; Fax: +83 53 950 6617; E-mail: shokim@knu.ac.kr

ions are of great importance for chemical, biological, and environmental research areas [7]. In this study, we have designed and prepared of new dye sensor and their heavy metal ions detection properties were examined and determined. Structure of the synthesized dye sensor was identified by ^{1}H-NMR, Mass and EA (elemental analysis). The metal ion sensing property of the dye sensor was determined by UV-Vis absorption behaviors and metal binding position was also investigated by computational calculation method, ^{1}H-NMR peak shift [8–13]. Electron density distribution and ^{1}H-NMR could provide the estimation of complex characteristic functions between electron rich interacting positions and electrophile metal ions. Furthermore, we also measured cyclicvoltammetry (CV) experiments to estimate the energy potentials, namely HOMO and LUMO. We have used the oxidation onset potential for calculation of HOMO energy levels and the UV absorption fit curve calculation of band gap energy for determined the corresponding LUMO energy levels. Finally, the complex formation types of metal detection were examined by Job's plot measurements [14–17].

2. Experimental

2.1. *Synthesis*

All the reagents and solvents, used for synthesis of azo chromophore dye sensor, were purchased from Aldrich and used without further purification. As presented in Scheme 1, precursor (a) synthesized by diazotization using NaNO$_2$ (60 mmol, 4.2 g) in the presence of HCl (54 ml) and 4-fluoroaniline (60 mmol, 6.7 g), the solution heat to 70°C. The solution was cooled to 0~5°C and stirred for 30 min. Second precursor (b) synthesized by salicylaldehyde (60 mmol, 6.4 ml) in 110 ml water containing 2.4 g NaOH and Na$_2$CO$_3$ 22.2 g the 5-Phenyldiazenyl salicylaldehyde dye (b) in good yields. 5-phenyldiazenyl salicylaldehyde (2 mmol, 0.488 g) and 4-phenylthiosemi carbazide (2 mmol, 0.334 g) were dissolved in 40 ml of ethanol. 3 drops
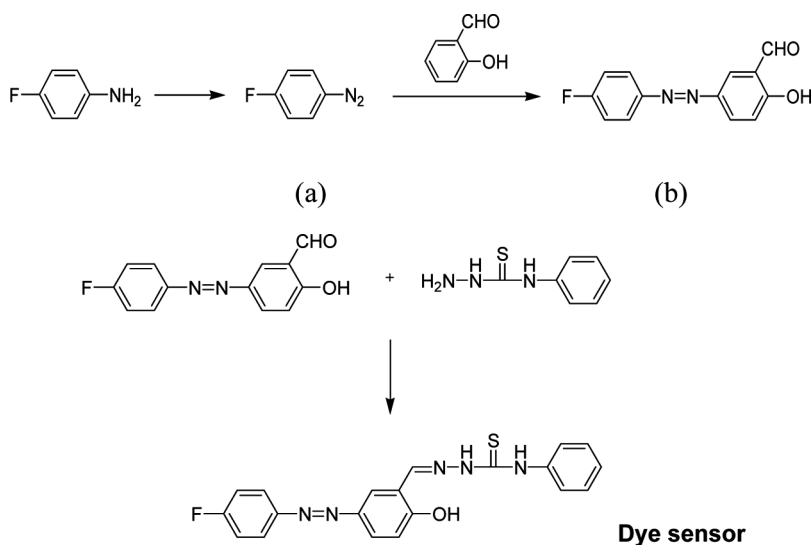
Scheme 1. Synthetic route for dye sensor.

of H_2SO_4 was added during the reaction. The reaction was continued for 7 h at room temperature. The reaction product was filtered and dried in the vacuum.

^{1}H-NMR (400MH$_Z$, DMSO-d$_6$) δ 11.85 (s, 1H), 10.93 (s, 1H), 10.22 (s, 1H), 8.72 (s, 1H), 8.54 (s, 1H), 7.88 (m, 2H), 7.78 (m, 1H), 7.52 (m, 2H), 7.38 (m, 4H), 7.18 (m, 1H), 7.04 (m, 1H). ^{13}C-NMR (DMSO-d$_6$) 176.0, 164.5, 162.1, 159.6, 148.8, 145.3, 139.2, 138.9, 128.0, 126.2, 125.4, 125.2, 124.5, 124.4, 122.5, 116.9, 116.4, 116.2, 40.1, 39.9, 39.7, 39.5, 39.2, 39.0, 38.8. MS: 393 (M$^+$). Anal. Calculated for $C_{20}H_{16}FN_5OS$: C, 61.06; H, 4.10; N, 17.80; S, 8.15: found; C, 63.28; H, 4.27; N, 18.04; S, 8.49.

2.2. *Measurements*

The spectroscopic characteristics of the prepared dye sensor were examined using Agilent 8453 UV-Vis spectrophotometer respectively. ^{1}H NMR spectra and elemental analyses were recorded with JNM-AL400 spectrometer operated at 400 MHz NMR and a Carlo Elba Model 1106 analyzer, respectively. Mass spectra were recorded on a Shimadzu QP-1000. HOMO/LUMO and electron distributions were calculated with Material Studio 4.3 [12,13]. Electrochemical properties were examined with Versa STAT3 using cyclicvoltammetry method. Cyclicvoltammetry measurement carried out in an acetonitrile solution containing tetrabutlyammonium hexafluorophosphate electrolyte. The reference electrode, Ag/Ag^+ was directly immersed in the reaction cell. The working electrode was a glassy carbon. The counter electrode was a platinum wire. The scan rate used 100 mV/s.

3. Results and Discussion

In this work, the dye sensor, 4-hydroxy-3-(fluoro-phenyl-thiourea-N'-nitrilo-methylidynyl)-azobenzene was prepared. UV-Vis absorption spectra were checked to determine the sensing functions of dye sensor toward various metal ions (Cd^{2+}, Hg^{2+}, Ni^{2+}, Zn^{2+}, Cu^{2+}, Fe^{3+} and Al^{3+}). The sensing investigations were conducted to Cd^{2+}, Hg^{2+}, Ni^{2+}, Zn^{2+}, Cu^{2+}, Fe^{3+} and Al^{3+} for dye sensor and the corresponding results were summarized in Figure 1. As shown in Figure 1, upon the addition of divalent metal ions to the solution of the prepared dye sensor, the absorption band at 331 nm progressively decreased and a new peak at 390 nm appeared. The appearance of this isosbestic point suggests that at least one stable dye sensor-divalent metal ion moiety is present. However, divalent metal ions showed the different isosbestic point at 357 nm and 361 nm. Namely, Cd^{2+} and Zn^{2+} were observed at 361 nm and Hg^{2+}, Ni^{2+} and Cu^{2+} indicate at 357 nm. We assumed that the absorption spectral changes are belonging to the different metal binding positions in dye sensor structure. This behavior causes significant increase in the charge density on the NH or S with associated enhancement in the push-pull effect of the mixture of intermolecular charge transfer (ICT).

The detection properties of dye sensor showed selectivity for metal ions especially divalent metal ions (Cd^{2+}, Hg^{2+}, Ni^{2+}, Zn^{2+} and Cu^{2+}). Other metal ions such as Fe^{3+}, Al^{3+} did not indicate the optical change. Dye sensor showed higher selective functions to Cu^{2+} ion, which resulted in great absorption enhancement at 390 nm. The detection properties for all applied metal ions were summarized in Figure 2.
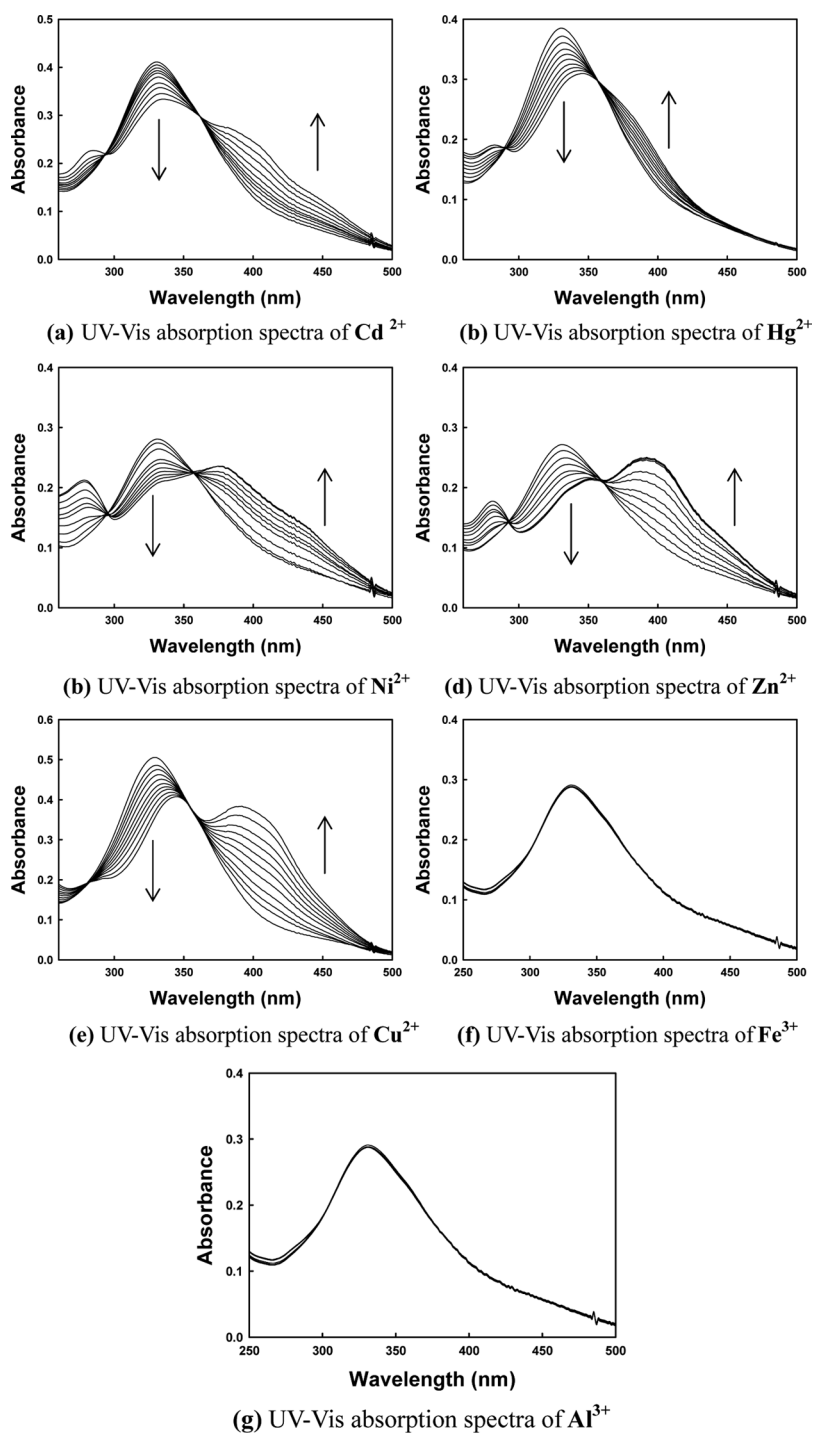
(a) UV-Vis absorption spectra of **Cd^{2+}**

(b) UV-Vis absorption spectra of **Hg^{2+}**

(b) UV-Vis absorption spectra of **Ni^{2+}**

(d) UV-Vis absorption spectra of **Zn^{2+}**

(e) UV-Vis absorption spectra of **Cu^{2+}**

(f) UV-Vis absorption spectra of **Fe^{3+}**

(g) UV-Vis absorption spectra of **Al^{3+}**

Figure 1. UV-Vis absorption spectra in the presence of 1×10^{-5} M of metal ions (Cd^{2+}, Hg^{2+}, Ni^{2+}, Zn^{2+}, Cu^{2+}, Fe^{3+} and Al^{3+}).
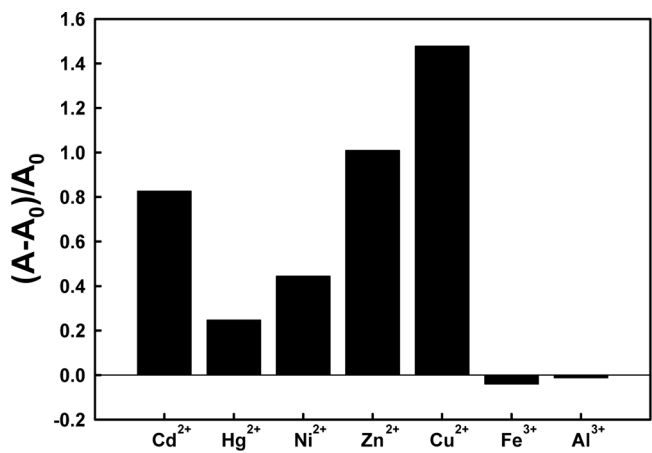
Figure 2. Comparison of absorption ratio for various metal ions (A and A_0 are the absorbance in the presence and the absence of metal ions, respectively at 390 nm).

Further to experimental determination of metal binding position, we estimated this binding property using the computational calculation and ^{1}H-NMR peak shift. Through computational calculation method, we calculated and determined the optimum molecular geometrical structure. In the Figure 3 showed that the optimization of molecular geometries structure and molecular orbital of dye sensor were
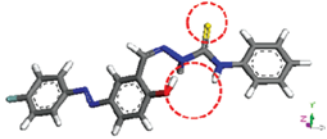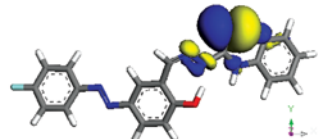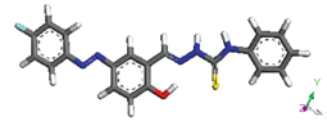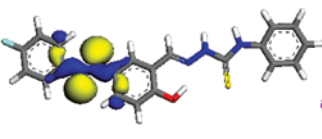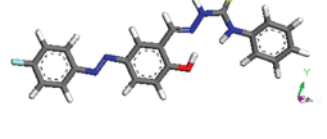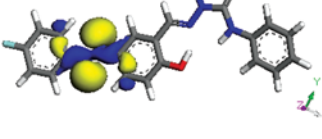

Figure 3. Geometry optimization: optimum structure and electron density distribution.

computationally optimized with various possible structures. Compared with HOMO/LUMO energy levels and energy gap, we selected the three structures. These three structures showed the different geometrical conformation. The resulting computational calculation indicated that the energy levels were HOMO/LUMO ($-5.110/-3.427$ eV), ΔE (1.683 eV) of structure (I), HOMO/LUMO ($-5.140/-3.115$ eV), ΔE (2.025 eV) of (II) and HOMO/LUMO ($-5.362/-3.365$ eV), ΔE (1.997 eV) of (III), respectively. The structure (I) indicates the lowest HOMO energy value and energy gap. In this reason, we proposed that the structure (I) is the most stabilized structure. In addition metal binding reactions could be made in electron rich HOMO state of dye sensor. Figure 3 clearly showed electron density of dye sensor that the electron density in HOMO was mainly localized in sulfur and -NH, where the possibility of metal binding reactions cab be expected.

To determine metal binding site using metal-ligand effects, we estimated the interaction of ligand with divalent metal ions (Zn^{2+} and Hg^{2+}) by ^{1}H-NMR shift behavior. Metal binding effects were observed in NMR peak shift of dye sensor in the presence of divalent metal ions. When the metal binding reaction occurred, these corresponding metal ions give an influence to the electron density distribution of dye sensor. Consequently, ^{1}H-NMR peaks were shifted due to different electron distribution.

It was found (Fig. 4) that the NH and OH proton signal on dye sensor (11.86 ppm, 10.22 ppm) disappeared with increasing the concentration of Hg^{2+} ion. And the upfield shift of the proton a in dye sensor was observed, which can be attributed to the increasing electron density. This behavior showed that Hg^{2+} ion could make efficient deprotonation of –NH and –OH of dye sensor. In contrast,
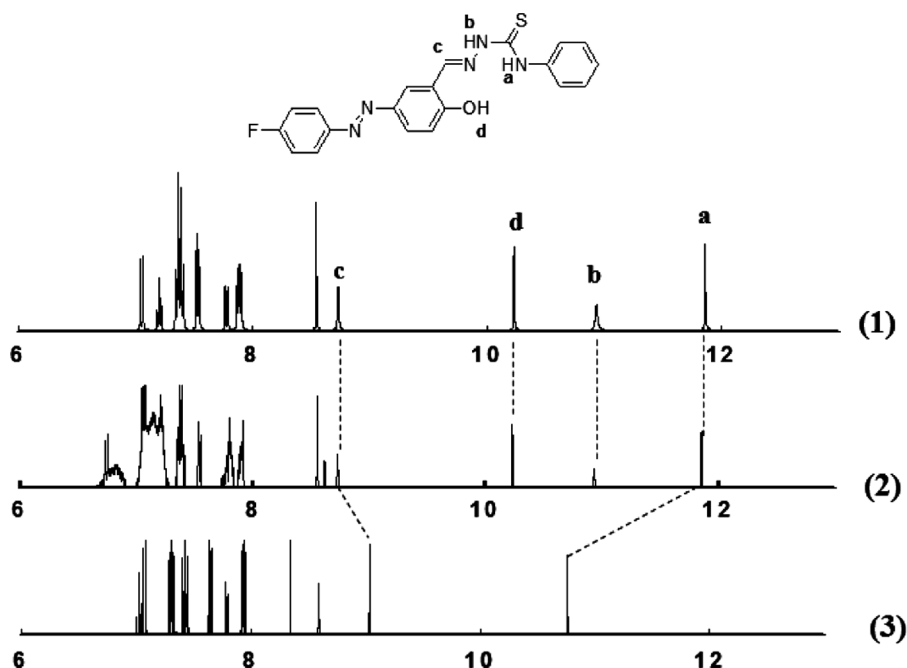

Figure 4. ^{1}H NMR changes of dye sensor in DMSO-d_6 (1) dye sensor, (2) and (3) in the presence of (2) Zn^{2+} and (3) Hg^{2+}.
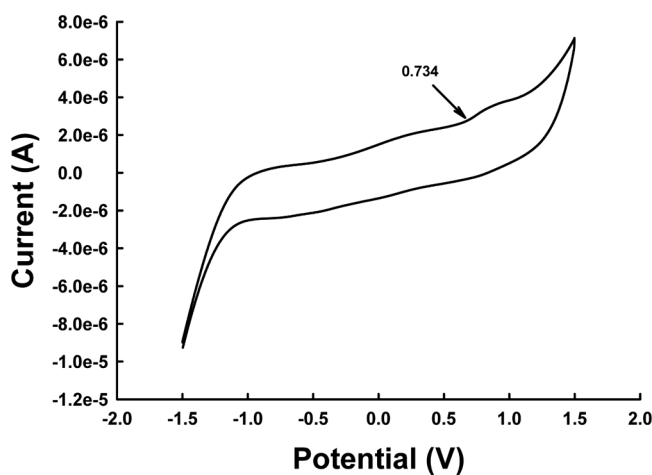
Figure 5. Cyclicvoltammogram of dye sensor in acetonitrile.

in the case of Zn^{2+}, the metal complexed dye sensor did not indicate the NMR peak shift. This behavior showed that Zn^{2+} metal biding position was not related to the deprotonation of –NH and –OH. If Zn^{2+} metal biding position was –NH or –OH, and then ^{1}H-NMR must show the peak shift. However, Zn^{2+} did not indicate any peak shift. Thus, we proposed that the metal binding positions of dye sensor were S and –NH. This behavior was well agreement with our expectation. Formally, we described the optimum structure of dye sensor with computational calculation. The optimum structure (I) showed that the sulfur atom formation was not influenced by other hydrogen. If optimum structure was (II) or (III), the peak shift can be monitored. In this reason, it can be proposed that this dye sensor had two metal binding positions as S and –NH.

Cyclicvoltammetric measurements of dye sensor were carried out in a conventional three-electrode system. The oxidation and reduction potential values were also used to estimate the HOMO/LUMO energy levels. Figure 5 showed the oxidation potential peak of dye sensor.

From the oxidation potential and UV fit curve, HOMO and LUMO energy levels of dye sensors were determined. HOMO and LUMO energy levels were calculated using the formula [18],

$$HOMO(orLUMO)(eV) = -4.8 - (E_{peak/onsetpotential} - E_{1/2}(Ferrocene))$$

Table 1. HOMO/LUMO values and energy gap of dye sensor

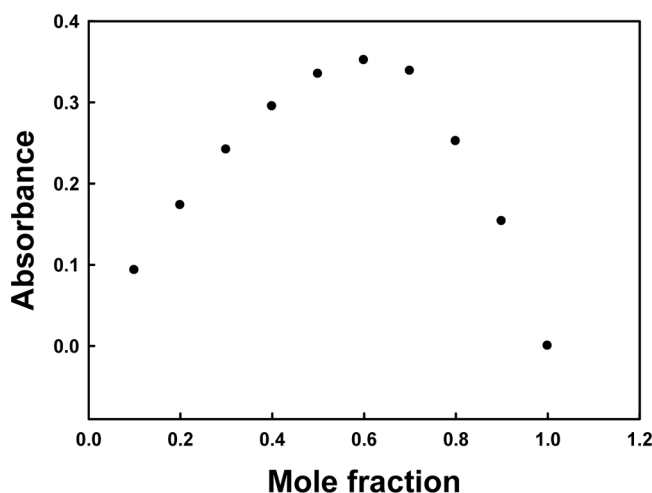|	Optimization structure			Cyclicvoltammetry and UV fit curve
	I	II	III	
HOMO	−5.110	−5.140	−5.362	−5.114
LUMO	−3.427	−3.115	−3.365	−2.189
ΔE	1.683	2.025	1.997	2.955

Figure 6. Plot of Job's method for dye sensor.

Where, $E_{peak/onset\ potential}$ are the maximum and minimum peak potential values and $E_{1/2(Ferrocene)}$ is half-wave potential of Ferrocene (0.42 V).

The comparison of computational calculation and experimental determination showed the similar values of HOMO/LUMO and ΔE (Table 1). Thus, the computational calculation results can be used as good supporting for the determination of metal binding reaction and position.

Finally, we determined the composition of the metal binding reaction using the Job's method [19]. For Job's plot measurements, 1×10^{-5} M solutions of dye sensor and different mole concentrations of metal ions were prepared in various molar
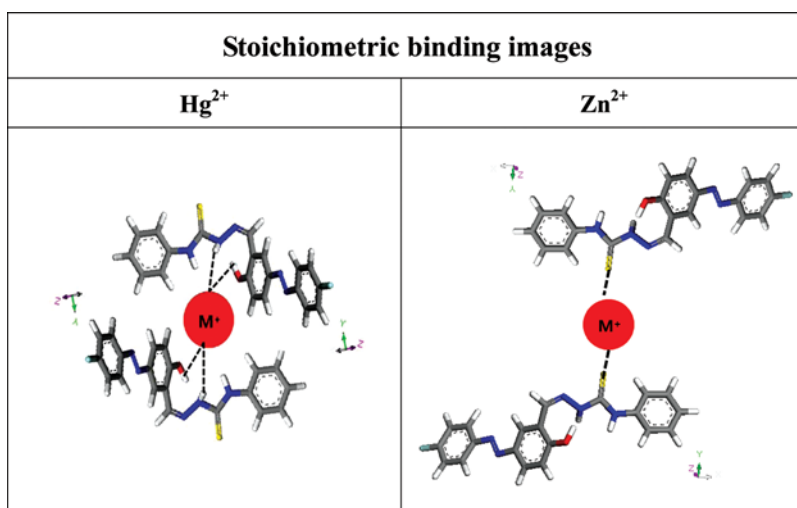

Figure 7. Stoichiometric binding images between dye sensor and divalent metal ion.

ratios of dye and metal ions (1:9, 2:8, 3:7, 4:6, 5:5, 6:4, 7:3, 8:2, 9:1, 10:0). The relationship for maximum absorption peak versus mole fraction of the metal ions is summarized in Figure 6. The finding exhibited that the molecular fraction was close to 0.6, which indicated 1:2 complex composition between metal ion and dye sensor. Electron density distribution, HOMO/LUMO energy level and ^{1}H-MNR result were considered to estimate the metal binding positions in dye sensor molecule (Fig. 7). In Figure 7, we propose stoichiometric binding images with two metal binding positions between dye sensor and divalent metal ions.

4. Conclusions

In this study, we investigated the effects of dye molecular chemosensing behaviors and metal binding position. It showed the metal detections properties of divalent metal ions. Especially, the dye sensor showed the divalent metal ion detection (Cd^{2+}, Hg^{2+}, Ni^{2+}, Zn^{2+} and Cu^{2+}). Other metal ions such as Fe^{3+} and Al^{3+} did not indicate the optical change. Especially, dye sensor showed higher selective functions to Cu^{2+} ion, which resulted in great absorption increase at 390 nm. The structure (I) showed the lowest HOMO energy value and energy gap. It is proposed that the structure (I) is the most stabilized structure where dye sensor-metal ion bindings are expected. The comparison of computational calculation and experimental determination showed the similar values of HOMO/LUMO and ΔE (Table 1). Furthermore, dye sensor-metal ion bindings were formed by M:L (1:2) stoichiometry complex type.

Acknowledgment

References

[1] Zhang, M., Lu, P., Ma, Y., & Shen, J. (2003). *J. Phys. Chem. B*, *107*, 6535.
[2] Yagi, S., Nakamura, S., Watanabe, D., & Nakazumi, H. (2009). *Dyes and Pigments*, *80*, 98.
[3] Wang, M. X., Meng, X. M., Zhu, M. Z., & Guo, Q. X. (2008). *Chinese Chemical Letters*, *19*, 977.
[4] Simionato, A. V. C., Cantu, M. D., & Carrilho, E. (2006). *Microchemical Journal*, *82*, 214.
[5] Song, K. C., Kim, M. H., Kim, H. J., & Chang, S. K. (2007). *Tetrahedron Letters*, *48*, 7464.
[6] Subodh, K., Prabhpreet, S., & Sukhdeep, K. (2007). *Tetrahedron*, *63*, 11724.
[7] Lehn, J. M. A. (1988). *Chem. Int. Ed. Engl.*, *27*, 89.
[8] Zhang, X., Ren, X., Xu, Q. H., Loh, K. P., & Chen, Z. K. (2009). *Org. Lett.*, *11*, 1257.
[9] Odabasoglu, M., Albayrak, C., Ozkanca, E., Aykan, F. Z., & Lonecke, P. (2007). *Journal of Molecular Structure*, *840*, 71.
[10] Ali, S. M., Maity, D. K., De, S., & Shenoi, M. R. K. (2008). *Desalination*, *232*, 181.
[11] Tang, J., Lian, N., He, X., & Zhang, G. (2008). *Journal of Molecular Structure*, *889*, 408.
[12] Delley, B. (1990). *J. Chem. Phys.*, *92*, 508.

[13] Tsutsui, S., Sakamoto, K., Yoshida, H., & Kunai, A. (2005). *J. Org. Met. Chem.*, *690*, 1324.
[14] Kim, D. W. (2002). *Polymer Science and Technology*, *13*, 101.
[15] Gritzner, G., & Kuta, J. (1984). *Pure & Appl. Chem.*, *56*, 461.
[16] Ni, Z., Shores, M. P. (2009). *J. Am. Chem. Soc.*, *131*, 32.
[17] Scheffe, J. R., Frances, A., King, D. M., Liang, X., Branch, B. A., Cavanagh, A. S., George, S. M., & Weimer, A. W. (2009). *Thin solid Films*, *517*, 1874.
[18] Lee, H. S., & Kim, J. H. (2007). *Polymer Science and Technology*, *18*, 488.
[19] Gibaud, S., Zirar, S. B., Mutzenhardt, P., Fries, I., & Astier, A. (2005). *International Journal of Pharmaceutics*, *306*, 107.